JOURNAL OF GEOPHYSICAL RESEARCH, VOL. 88, NO. A9, PAGES 7037–7050, SEPTEMBER 1, 1983

Energetic Electron Precipitation Due to Gyroresonant Interactions in the Magnetosphere Involving Coherent VLF Waves With Slowly Varying Frequency

H. C. CHANG, U. S. INAN, AND T. F. BELL

Space, Telecommunications and Radioscience Laboratory, Stanford University, Stanford, California 94305

A test particle simulation model (Inan et al., 1982) of the gyroresonance wave-particle interaction in the magnetosphere is extended to study the transient particle precipitation fluxes induced by various coherent VLF waves with slowly varying frequency propagating along the earth's magnetic field lines. For moderate wave intensities ($B_w \leq 10$ pT at L=4) a comparison between input signals with linearly rising and falling frequencies shows that they induce the same amount of precipitated particle energy deposition. However, when the wave growth near the principal interaction region is considered, the precipitation induced by a riser is considerably higher than that induced by a faller. The effect of the frequency-time slope (df/dt) of the input signal on the induced precipitation energy flux is found to be small. Our results indicate, however, that the precipitation energy flux depends strongly on the falloff in energy of the trapped particle distribution function. The model is applied for computing the transient precipitation energy fluxes induced by a triggered rising emission, a hooklike signal and a one-hop whistler. The total precipitated energy deposition for these various signals is found to be comparable to that induced by a linear ramp having the same input wave energy density.

1. INTRODUCTION

In this paper we study the precipitation of energetic electrons into the ionosphere due to pitch angle scattering of these particles by coherent variable frequency VLF wave packets in the magnetosphere. The waves and the particles are assumed to interact in the cyclotron resonance mode [*Inan et al.*, 1978].

Recently, a number of observations of electron precipitation have been attributed to naturally occurring transient VLF waves, including lightning-generated whistlers and chorus emissions [*Rosenberg et al.*, 1971; *Helliwell et al.*, 1973; *Foster and Rosenberg*, 1976; *Helliwell et al.*, 1980; *Rosenberg et al.*, 1981; *Dingle and Carpenter*, 1981; *Carpenter and LaBelle*, 1982]. Moreover, it has been suggested that observed narrow peaks in the energy spectra of electrons precipitating from the inner radiation belt originate from interactions with ground-based transmitter signals [*Vampola and Kuck*, 1978; *Koons et al.*, 1981; *Imhof et al.*, 1981*a*, *b*] and the first direct observation of energetic electrons precipitated by these signals has recently been reported [*Imhof et al.*, 1983].

Natural whistlers, chorus emissions, triggered emissions, and some of the signals from ground-based VLF transmitters are examples of coherent variable frequency waves in the magnetosphere. This paper provides a basis for the study of particle precipitation related to these more general cases of whistler mode waves with slowly varying frequency.

Precipitation of the radiation belt particles is but one result of the gyroresonance interactions in the magnetosphere between energetic particles and waves. Particles can undergo large pitch angle changes by resonating with the coherent wave over distances of many hundred wavelengths [*Inan et al.*, 1978]. This process is fundamentally different from that involving incoherent signals, such as plasmaspheric hiss, in which the particles execute a random walk in velocity space [*Roberts*, 1966]. In this paper we deal with coherent signals.

As it propagates along the earth's magnetic field line between the two hemispheres, a variable frequency wave pulse can interact with particles of different energy and pitch angle for which the cyclotron resonance condition is locally satisfied. The nonlinear trajectories of particles under the influence of monochromatic waves have been studied in detail by *Inan et al.* [1978] using a test particle simulation approach. This simulation model has recently been extended to higher energies by including relativistic effects [*Chang and Inan*, 1983]. In this study we employ a simulation of the interaction of a large number of test particles with a given wave. The particles are from an assumed initial trapped distribution and continually enter the wave packet through the leading edge of the propagating wave pulse. By taking account of the group travel times of wave components of different frequency and the particle travel times, we compute the temporal variation of the resulting precipitated energy flux as a function of time.

In this paper we extend and generalize a recent study of the transient particle precipitation induced by a short-duration monochromatic VLF wave (*Inan et al.* [1982], hereinafter referred to to as [*I*]). The method of computation as well as much of the background and justification for the present work are given by [*I*]. Here we concentrate on extending the method to the case of interactions involving variable frequency wave pulses.

In section 2 we first investigate the cyclotron resonance conditions for a wave pulse with slowly varying frequency as it propagates in the dispersive magnetospheric medium. After formulating the problem in section 3, we compare in section 4 the precipitation induced by a linear riser and faller and discuss the possible implications of signal amplification. Input signals of different frequency-time format are studied

Paper number 3A0657.
0148-0227/83/003A-0657$05.00

in section 5. Finally, in section 6 we estimate the transient precipitation fluxes induced by a rising emission, a hook, and a lightning-generated one-hop whistler.

2. Cyclotron Resonance Velocity

In this section we bring to light the differences between monochromatic waves and waves with slowly varying frequency, from the point of view of the resonance locations along the field line. We consider a longitudinally propagating whistler mode wave whose amplitude B_w, wave number k, and frequency ω all vary slowly within 2π period of the wave phase (e.g., $\Delta\omega/\omega < 1\%$ within one wave cycle). With ϕ defined as the angle between the perpendicular (to the field line) velocity $\mathbf{v}_\perp$ of a particle and $-\mathbf{B}_w$, the variation of ϕ due to the influence of the wave and the adiabatic motion of the particle can be expressed [*Dysthe*, 1971; *Inan et al.*, 1978] as

$$\dot{\phi} = \omega_H - \omega - kv_{\parallel} - \frac{eB_w}{m}(v_{\parallel} + \frac{\omega}{k})\frac{\cos\phi}{v_\perp} \quad (1)$$

where $\omega_H = eB_0/m$ is the angular gyrofrequency and $v_{\parallel}$, e, and m are the parallel velocity, charge, and mass of the electron, respectively. The directions of $\mathbf{v}_{\parallel}$ and $\mathbf{k}$ are as shown in Figure 1*a*. It can be shown [*Inan, 1977*] that for the typical parameters of interest the last term on the right-hand side in (1) is neglibible unless $v_\perp \to 0$. Neglecting this last term and defining the cyclotron resonance velocity as

$$v_R = \frac{\omega_H - \omega}{k} \quad (2)$$

we can rewrite (1) as

$$\dot{\phi} = k(v_R - v_{\parallel}) \quad (3)$$

For typical magnetospheric conditions, $B_w/B_0 \ll 1$, and the wave-induced perturbations in the adiabatic trajectory of the particle are cumulative only when the following cyclotron resonance condition is satisfied:

$$v_{\parallel} \simeq v_R = (\omega_H - \omega)/k \quad (4)$$

Note that (4) for the whistler mode ($\omega < \omega_H$) can only be satisfied when the particles and the wave travel in opposite directions.

In Figure 1*b* we plot the resonance velocity v_R as the dashed curve, assuming a continuous wave of constant frequency f_2 along the field line. For this case, v_R is symmetric around the equator due to the symmetry of the local ω_H and k for the assumed dipole model of the magnetic field and diffusive equilibrium model for the cold plasma. Also shown as a dotted line in Figure 1*b* is the adiabatic parallel velocity $v_{\parallel}$ of a particle, also symmetric around the equator. Note that the latter is a function of the particle energy and pitch angle as determined by the first adiabatic invariant [*Roederer*, 1970]. For the case when the v_R and $v_{\parallel}$ curves are tangent to each other, the particle resonates with the wave at the equator. For other particles there exist two intersection points as indicated in Figure 1*b*, meaning that the cyclotron resonance condition is satisfied in the vicinity of two conjugate locations along the field line. The strongest interaction takes place when the interaction point is at the equator in which case $\ddot{\phi} \simeq 0$.

We now review the interaction for the case of a short fixed frequency pulse. As shown in Figure 1 a short pulse of duration t_{PL} and fixed frequency f_2 is taken to be propagating from south to north along the field line. The two boxes in Figure 1*a* represent the portions of the field line occupied by the wave packet at times t_1 and t_2. Here we neglect the possible stretching and distortion of the front and tail ends of the pulse [*Chang and Helliwell*, 1980], since the amount of such stretching is much shorter than the pulse durations being considered in this paper. The corresponding portions of the resonance velocity curve as defined by the locations of the pulse front and tail at times t_1 and t_2, respectively, are shown by the two boxes in Figure 1*b*.

Now consider a particle which encounters the front end of the wave packet at the equator and at time t_1. The solid segment which starts at the equator and ends at the point at which the particle exits the wave packet represents the resonance velocity curve as 'observed' by this particle. Note that the exit point is different from the location of the tail end of the pulse at time t_1, owing to the relative motion of the particle and the wave. The point of resonance for a given particle will then be at the intersection (if any) of the adiabatic parallel velocity curve for that particle and this solid segment. The other solid curve in Figure 1*b* is the resonance velocity curve seen by another particle which encounters the wave packet at time t_2.

Note that for a monochromatic wave the resonance velocity segment observed by any particle that travels through the wave packet always lies on the dashed line in Figure 1*b*. Thus for that particle whose adiabatic $v_{\parallel}$ is shown in Figure 1*b*, the point of intersection between the $v_{\parallel}$ curve and the v_R segment determines the point of resonance if

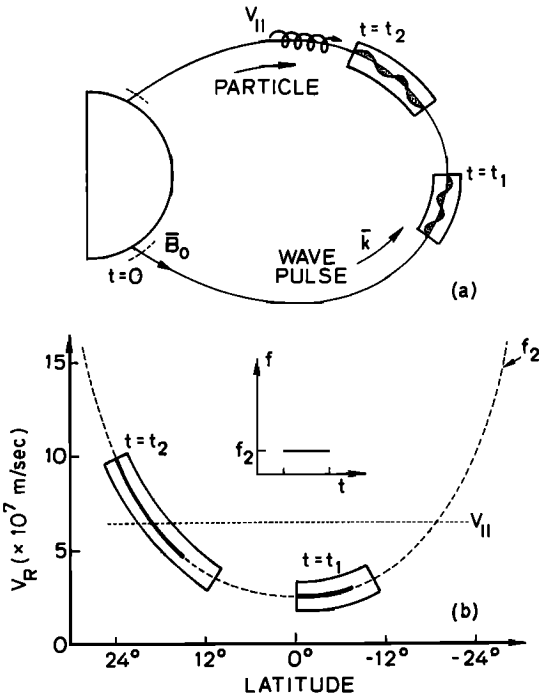

Fig. 1. (*a*) Schematic describing the motion of the particle and a wave pulse. The two boxes represent the portions of the field line occupied by the wave packet at times t_1 and t_2. (*b*) The dashed curve shows the resonance velocity v_R for a constant frequency f_2. The dotted curve gives the adiabatic parallel velocity of a particle. The solid segments represent the v_R curves as observed by the particle as it encounters the front end of the wave packet at time t_1 and t_2, respectively.

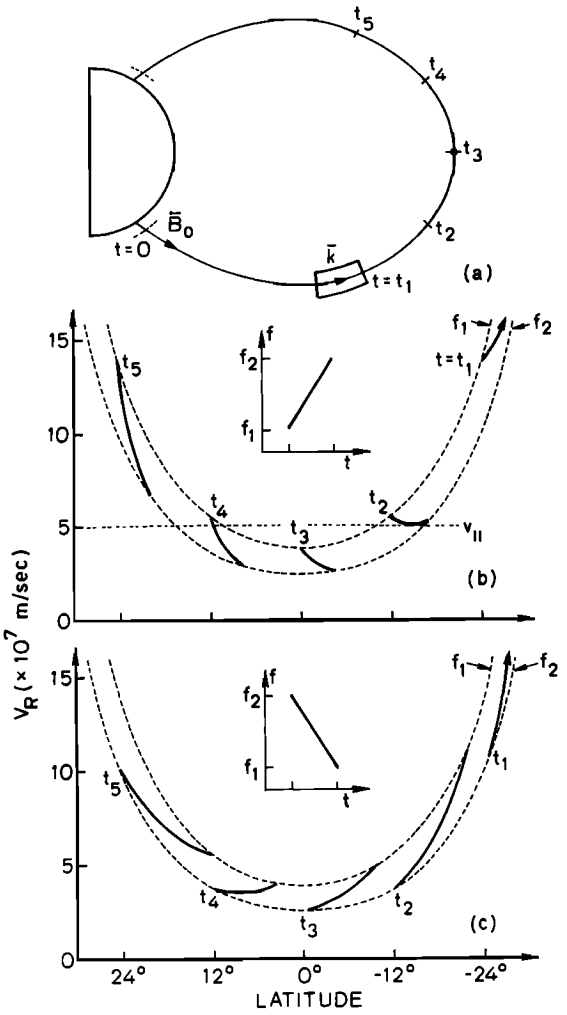

Fig. 2. (*a*) Locations along the field line of the front end of a variable-frequency wave packet at times t_i, i=1, ···, 5. (*b*) and (*c*) Typical v_R curves for the case of a linear ramp with rising frequency from f_1 to f_2 and for the case of a linear ramp with falling frequency from f_2 to f_1, respectively. The dashed curves are the v_R curves for constant frequencies f_1 and f_2. In (*b*) is shown an adiabatic parallel velocity curve of a particle tangent to one v_R curve.

this particle encounters the front end of the pulse at time t_2. However, the cumulative scattering experienced by this particle will be negligible if this particle encounters the pulse front at time t_1, since at that point it is far from being close to resonance.

We now apply these concepts to the more complicated cases of interactions with wave pulses having slowly varying frequency. Figure 2 shows two such cases, a riser and a faller. Both signals have the same intial pulse duration t_{PL} and the same upper and lower frequencies with an input $f-t$ format that varies linearly in frequency when observed at the injection point into the magnetosphere. Note that the $f-t$ format varies along the field line due to the dispersion of the signal. This variation has been taken into account in the following.

The two dashed curves in Figures 2*a* and 2*b* show v_R for constant frequency waves with frequencies f_1 and f_2, respectively. Each segment in Figure 2*b* represents the characteristic resonance velocity curve seen by a particular particle that enters the wave packet at time t_i ($i = 1, 2, \cdots, 5$) at the corresponding latitude along the field line. The segments start at the f_1 curve and end at the f_2 curve, since f_1 and f_2 are the frequencies of the front and tail ends of the wave pulse, respectively. Particles of different velocities encounter a specific frequency component of the wave pulse at different positions during their relative motion with respect to the wave packet. Thus v_R, which is determined by the wave frequency variation experienced by the particle along the field line, is different for different particles that encounter the wave at a given time. In Figure 2*c* we show v_R for the case of a faller. Note that the resonance velocity segments start at f_2 and end at f_1 in this case.

The strongest interaction between the wave and the particles takes place when the resonance point is located in the neighborhood of the point where the gradient of the resonance velocity vanishes. This occurs at the geomagnetic equator for a constant frequency wave. *Helliwell* [1970] has shown that the strongest resonance point for a variable frequency wave is located off the equator at a position (termed the 'phase equator') where the spatial variation of the electron gyrofrequency is matched to the spatial variation of the doppler-shifted wave frequency seen by the particle. In the context of Figure 2 this is represented by the point of tangency between $v_{||}$ (dotted curve) and v_R curves and (especially for the low pitch angle particles) is located very close to the zero gradient point of the v_R curve. Although the resonance velocity is different for different particles, this point of strongest interaction can be roughly defined by some representative v_R curves. For example, in Figure 2*b* the resonance point will be located between the positions of the leading edge of the pulse at times t_1 and t_2, since the v_R curve of a particle which meets the pulse front at $t = t_2$ shows a local minimum. On the other hand, for the faller as shown in Figure 2*c* this point is located on the other side of the equator. The neighborhood of this point will hereinafter be called the 'principal interaction region,' within which the variations of local gyrofrequency and wave frequency as seen by the resonant particle are quasibalanced, and the particle experiences an unperturbed phase variation similar to that of a particle resonating with a monochromatic wave near the geomagnetic equator [*Helliwell*, 1970].

3. Parameters, Models, and Formulation of Problem

For the results given in the following sections, the wave pulses are considered to originate in a model magnetosphere at 1000 km altitude in the southern hemisphere at $t = 0$. We consider interactions on the L=4 field line with an equatorial electron density of 400 el/cm^3 and a diffusive equilibrium model for the cold plasma distribution [*Angerami and Carpenter*, 1966]. The different types of wave pulses considered are normalized to have an input power density of 1.67×10^{-8} W/m^2 corresponding to that of a fixed frequency wave at half the equatorial gyrofrequency (6.8 kHz at L=4) with magnetic field intensity of 5 pT at the equatorial plane, except for cases in which we discuss wave amplification.

As the input wave pulse propagates northward along the field line, it interacts with energetic particles for which the cyclotron resonance condition (4) is locally satisfied and some of these particles may be precipitated out of the radia-

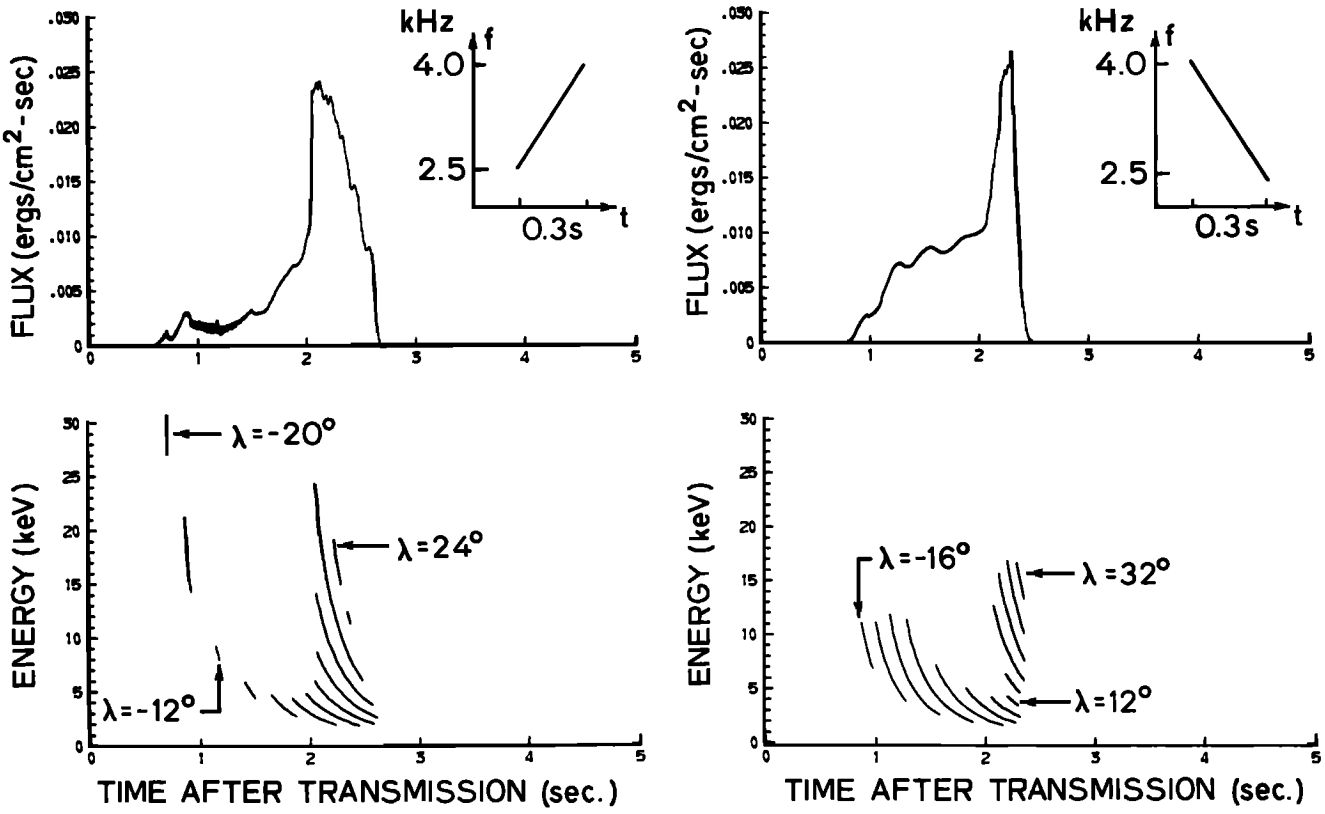

Fig. 3. The top panels show the transient precipitated energy fluxes versus time after the injection of the wave into the magnetosphere at 1000 km altitude for a riser and faller, respectively, with their input formats given in the $f - t$ domain. The bottom panels show the energy of the particles that constitute the corresponding fluxes.

tion belts. Particles are considered to be precipitated if their equatorial pitch angle after interacting with the wave is smaller than the half angle of the equatorial loss cone within which the population of the energetic particles is assumed to be zero before the injection of the wave pulse. In our model computation and for the wave intensities considered, test particles that are scattered in equatorial pitch angle by 0.1° are considered. In other words, particles for which $\Delta\alpha_{eq} < 0.1°$, where α_{eq} is the equatorial pitch angle, are assumed to be not effected by the wave.

The initial unperturbed distribution function of the trapped particles is assumed to be of the form [*Inan et al.*, 1978, 1982]:

$$f(v,\alpha) = Av^{-n}g(\alpha) \qquad \alpha \geq \alpha_{lc}$$
$$f(v,\alpha) = 0 \qquad \alpha < \alpha_{lc} \tag{5}$$

where A is a constant, n is an exponent that can be adjusted to fit observed distributions, $g(\alpha)$ is some function of pitch angle and α_{lc} is the angular halfwidth of the loss cone. For the purposes of this paper $f(v,\alpha)$ has been assumed to be isotropic ($g(\alpha) = 1$) and A has been chosen such that the differential energy spectrum for electrons with 1 keV energy is $\Phi_E = 10^8$ el/cm^2 ster s keV. In most of the cases, n in (5) has been chosen to be 6. It should be noted that in the magnetosphere the value of Φ_E can vary between 10^6–10^8 el/cm^2 ster s keV [*Lyons and Williams*, 1975]. The precipitated energy fluxes computed in our model are directly proportional to Φ_E. Thus the energy flux values given in Figures 3–14 can simply be linearly scaled in accordance with the value of Φ_E for the particular case under consideration.

Since we adopt the same formulation and method of computation as those employed by [*I*] for interactions with fixed frequency wave pulses, the details will not be repeated here. Our formulation accounts for the fact that the leading edge of the wave pulse continually encounters new distributions of particles as the wave packet propagates. Taking into account the wave and particle travel times, the precipitation due to the encounter of each such distribution of incoming particles with the wave pulse is superposed to obtain the precipitated energy flux as a function of time that would be observed at the injection point of the wave.

Owing to the dispersive nature of the magnetospheric medium, the temporal duration of a variable frequency wave packet changes as it propagates along the field line. Due to the conservation of energy the power density and the magnetic field intensity of a propagating wave pulse will thus vary along the field line in accordance with the variation of the instantaneous pulse duration, the local cross-sectional area of the duct to which the energy is assumed to be confined, and the local refractive index. Details of these properties are discussed in the appendix. In our calculations we have taken full account of these pulse duration and wave amplitude variation effects. Indeed, these effects are found to be essential in the correct interpretation of the results presented in the following sections.

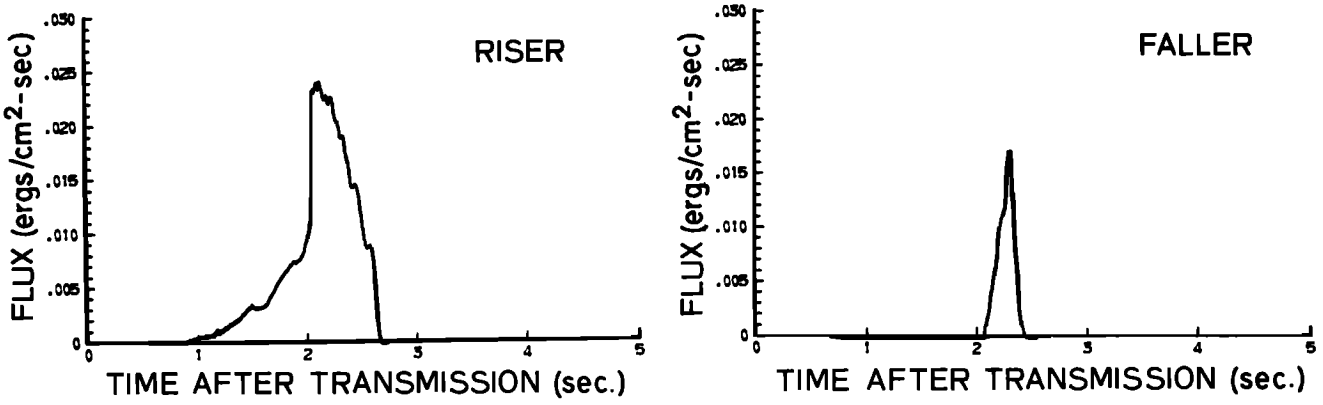

Fig. 4. The precipitated energy fluxes for the same input signal formats as in Figure 3 except that a 20-dB wave growth near the principal interaction region is taken into account.

4. Precipitation Induced by Riser and Faller

We now consider two input wave pulses with linearly rising and falling frequencies, the formats of which are shown in the upper panels of Figure 3. Both pulses have the same initial duration of 0.3 s and upper and lower frequencies of 4.0 kHz and 2.5 kHz, respectively. These two signals were taken to have the same input power; however, they have different equatorial wave intensities, as discussed in the appendix.

The upper panels of Figure 3 show the precipitated energy fluxes versus time induced by the riser and faller, assuming n=6 in (5). The lower panels show the energy ranges and arrival times at the ionosphere of the particles constituting these downcoming fluxes. The energy range of the precipitating electrons arriving at any time t can be defined by the upper and lower bounds of all of the curve segments at that time. These lower panels are termed 'energy diagrams' and are further explained below.

As the leading edge of the wave pulse arrives at a given latitude on the field line, it encounters an unperturbed distribution of energetic particles; however, only particles within some limited range of energy can be scattered into the loss cone and precipitate into the ionosphere. Each curve in the energy diagram then represents this precipitating energy range versus arrival time for a specific location of the pulse front. For example, in the case of the riser, the leftmost curve corresponds to the case when the pulse front is at $-20°$ latitude ($\lambda = -20°$) and each following curve accounts for a $4°$ increase in latitude until the pulse front reaches $\lambda = 24°$. As the pulse travels up the field line, the curve shifts to the right in the diagram due to the increased group delay of the wave packet and the travel time for particles. The energy curves for the faller in the lower right panel of Figure 3 are shown from $\lambda = -16°$ to $32°$ latitude with a $4°$ step.

The shortest segments in the energy diagram, marked $\lambda = -12°$ for the riser and $\lambda = +12°$ for the faller, represent the steps when the front end of the pulse is within the principal interaction region as defined in section 2. The fact that it has the narrowest energy range can be understood from Figure 2; the range in particle parallel velocity of the $v_{\|}$ curves which could have points of intersection with the v_R curve is the smallest for the step around the principal interaction region.

We can infer from Figure 3 how particles interacting with the wave at different locations contribute to the time evolution of the precipitated fluxes. Both of the responses are composed of two parts, a high-flux region around the peak and a lower flux region which arrives earlier. The occurrence of a high-flux or peak portion is due to the accumulation of downcoming particles in a relatively wide energy range, as can be understood from the energy curves. In the case of the faller the energy range corresponding to the lower flux portion is narrower than that corresponding to the peak part. This range is even smaller for the case of the riser, thus accounting for the low flux level in the leading part of the precipitation pulse.

The total precipitated energy density obtained by integrating the flux over time is the same for the two cases shown in Figure 3. This can be understood on the basis of the fact that both pulses have the same input energy density and the same frequency range, so that they interact with the same ranges of energetic electrons along the field line. It should be noted that this result would not have been obtained if we had not included the wave amplitude variation due to the dispersion of the wave pulse, as discussed in the appendix.

We have already discussed the locations of the principal interaction regions for variable frequency cases. Referring to Figure 3, for the riser the precipitation flux resulting from the interactions near the principal interaction region is significantly lower than that of the main portion of the precipitation pulse. However, for the faller the interactions near the principal interaction region constitute part of the peak flux.

The results of Figure 3 were obtained by assuming that the total energy density of the propagating pulse is constant everywhere on the field line, i.e., that there is neither wave damping nor growth. It is generally believed that the amplification or growth of monochromatic VLF waves takes place near the geomagnetic equatorial plane. By employing the same physical reasoning, the amplification of variable frequency signals would take place around the phase equator or the principal interaction region [*Helliwell*, 1967; 1970]. As long as the pulse is long enough (300 ms in this case) such that there is time for the particles to be phase bunched, the input wave might be amplified up to 30 dB as it traverses the principal interaction region [*Helliwell and Katsufrakis*, 1974]. To study these cases we have computed the precipitation

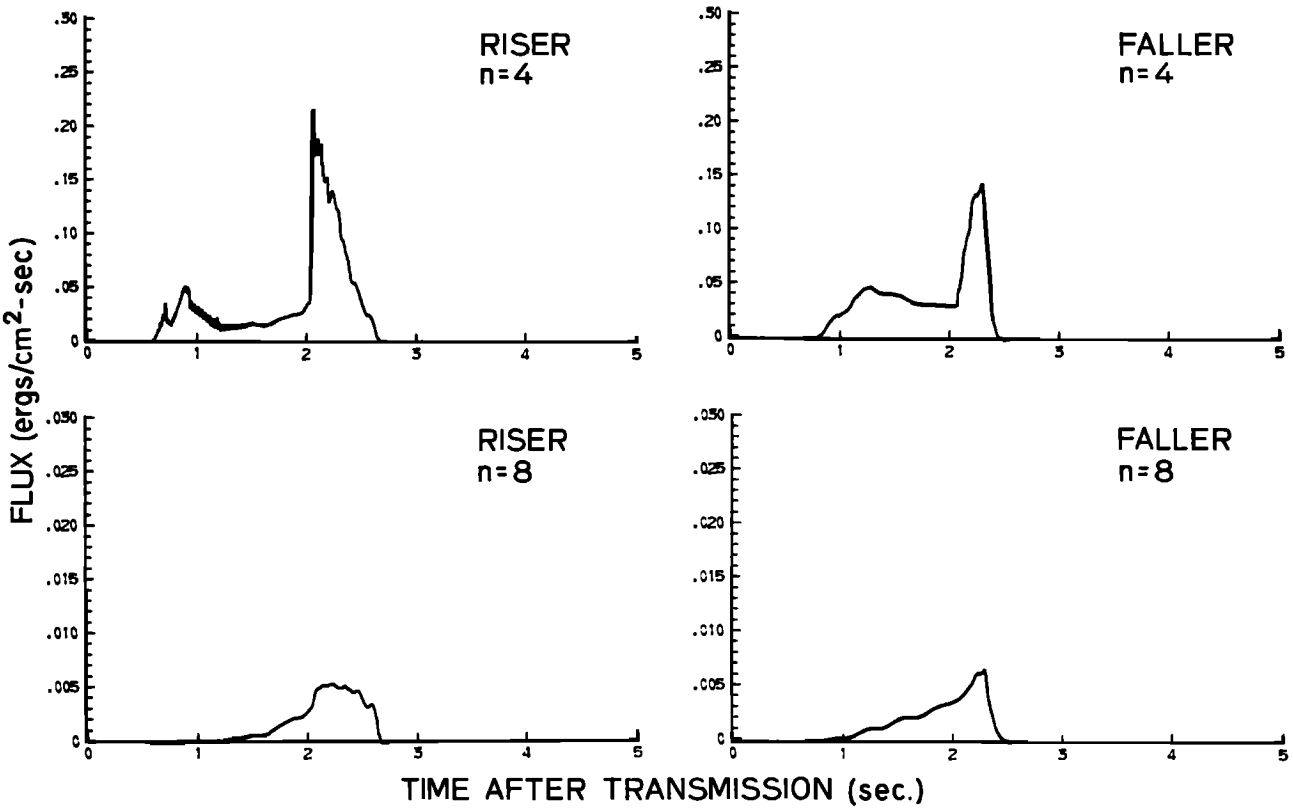

Fig. 5. Precipitated energy fluxes versus time for the same input signals as in Figure 3 and for n=4 and n=8 distributions. Other parameters are the same as those of Figure 3.

due to amplified waves, and the results are shown in Figure 4. The parameters and assumptions used are the same as those used in Figure 3 except that the wave intensity is assumed to be 20 dB lower prior to the wave's traversal of the principal interaction region. Thus the energy density in the pulses in Figure 3 and 4 is the same after they pass the principal interaction region, while the input power is 20 dB lower in Figure 4 than that assumed in Figure 3.

For the riser case given in the left panel in Figure 4, only a small portion in the leading edge of the transient precipitation pulse is reduced from that given in Figure 3. However, for the faller in the right panel, both the peak flux level and the width in time of the response are significantly reduced in comparison with that in Figure 3. The response of the faller between $t = 1$ s and $t = 2$ s is shown to be zero because the pitch angle scattering induced by the 20 dB lower signal is smaller than the resolution ($\Delta\alpha_{eq} = 0.1°$) employed in the computer calculations.

The results of Figure 4 imply that a signal with rising frequency would be more efficient than one with falling frequency in inducing particle precipitation in situations in which signal growth might be present. Note that the same would apply in cases of natural chorus emissions that may be spontaneously generated in the vicinity of the principal interaction region.

The results shown in Figures 3 and 4 are for a trapped particle distribution function with n=6 in (5). To demonstrate the role of this parameter, we show in Figure 5 precipitated flux versus time for n=4 and n=8. Other parameters of Figure 5 are the same as those of Figure 3. We have normalized the trapped distribution function to a fixed Φ_E at E=1 keV so the population of the energetic particles above 1 keV will be larger for lower n values. In Figure 5 the flux scale for the n=4 cases is chosen to be one order of magnitude larger than for the n=6 cases, while that for the n=8 cases is the same as in Figure 3.

For the n=4 distribution the contribution of the higher energy particles to the precipitation is more important than for the $n = 6$ case. This can be understood from the fact that there is a significant drop in flux near the center of the precipitation pulse for both riser and faller, as shown in the top panels of Figure 5. The low flux part is associated with the lower energy particles which interact with the wave pulse near the geomagnetic equatorial plane (see Figure 3). Consequently, the peak and the early-arriving portions of the transient precipitation pulse become better defined for cases of lower n value. In contrast, the results for the n=8 distribution as given in the bottom panels in Figure 5 show a smoother temporal variation, since the contributions of the lower energy particles are relatively more important for distribution functions with higher n. Therefore the peak flux is less dominant in such cases.

5. Effect of df/dt

In this section we demonstrate the dependence of the precipitated flux on the frequency-time slope of the input signal. The formats (at 1000 km altitude) of the input pulses selected are shown in Figure 6 and are separated into three categories: (a) pulses with the same frequency range but of different initial duration (i.e., temporal duration observed at 1000 km altitude), (b) pulses of the same initial duration

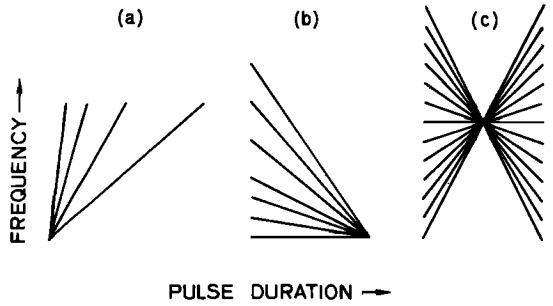

Fig. 6. Formats of the input pulses used in the study of the effect of df/dt on the particle precipitation.

but with varying upper frequency, and (c) pulses of the same initial duration and center frequency but with varying slope. The input power of each pulse has been taken the same as defined earlier; the total energy in the pulse is then proportional to the input pulse duration.

Dependence on Input Pulse Duration

Figure 7 shows the precipitation fluxes due to pulses of different input duration as shown in Figure 6*a*. The upper and lower frequencies of these pulses were taken to be the same, namely, 6.8 kHz and 5.1 kHz ($\Lambda \equiv f/f_{H_{eq}}=1/2$ and 3/8, respectively). The $f-t$ slopes of these input signals vary from 4.25 kHz/s up to 34 kHz/s for the pulse durations of 0.4 s to 0.05 s that are considered. The energetic particle distribution function is assumed to be as in (5) with $n=6$.

Since all signals considered cover the same frequency range, they interact with particles in the same energy range as they propagate along the field line. This is also evident from the fact that each precipitation pulse spans about the same range in time, namely, 1 to 4 s after $t=0$. Note that the arrival times and the duration of the precipitated flux are essentially determined by the wave and particle travel times along the field line.

Figure 7 shows that the peak flux level as well as the integrated energy density decrease as the pulse duration is reduced. This is mainly due to the reduced interaction length (defined as the distance over which the particle parallel velocity stays within a few percent of the local resonance velocity) for individual particles, as can be understood from Figures 1 and 2. The effect of pulse duration on the particle precipitation discussed here is basically similar to that for the constant frequency pulses as discussed by [*1*], where it was shown that the precipitated energy flux increases with pulse length while the precipitation pulses are of about the same temporal duration.

Dependence on the Frequency Range

Next we consider the fixed duration pulses shown in Figure 6*b*. Note that as compared to those of Figure 6*a*, these pulses have the same input power and total energy. In Figure 8 we compare the various pulses on the basis of the peak flux F_P and the integrated energy density E_T (in ergs per square centimeter), two quantities which were shown by [*1*] to approximately characterize the transient precipitation pulse.

We show the results for three different distributions, namely $n=4$, 6, and 8. For $n=6$ and 8, F_P and E_T increase with increasing upper frequency of the input wave, while

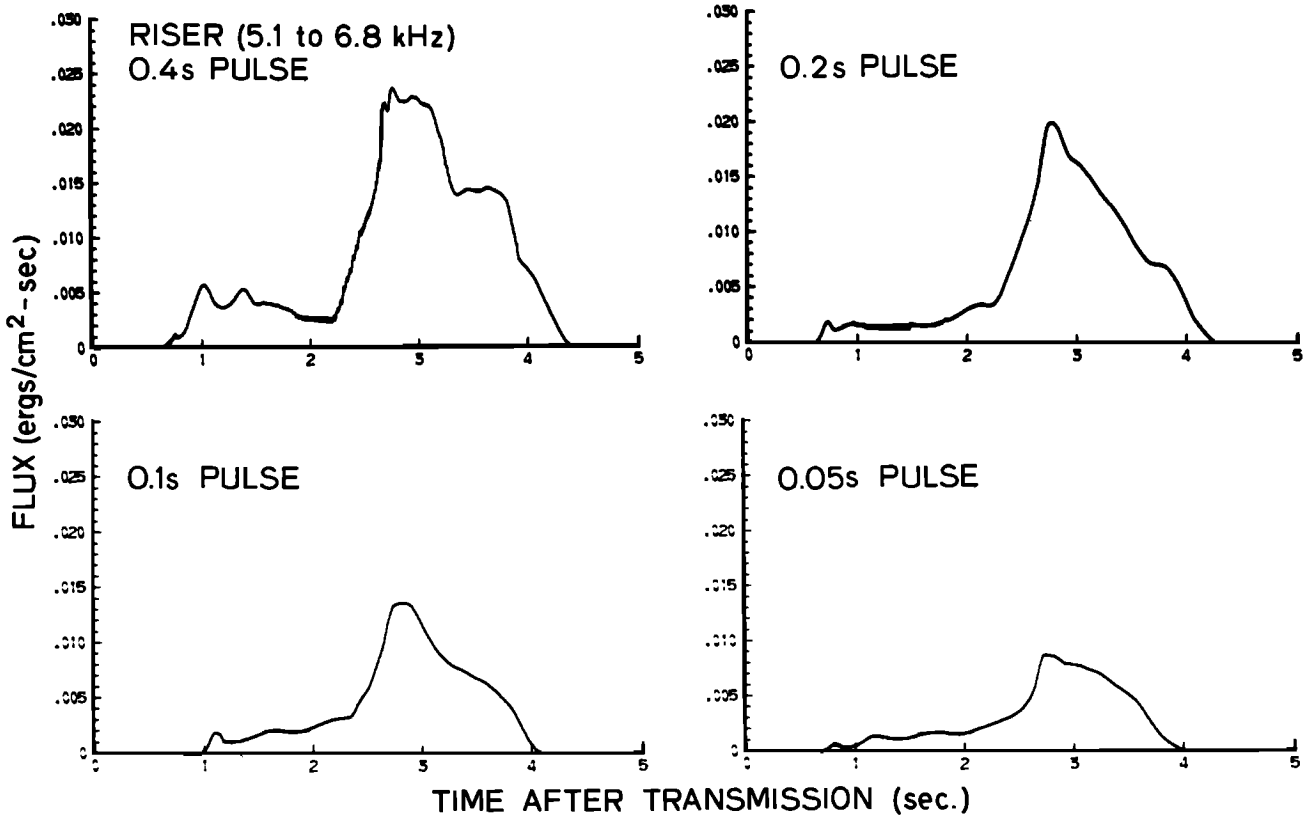

Fig. 7. Precipitated energy fluxes versus time for signals whose input formats are given in Figure 6*a*.

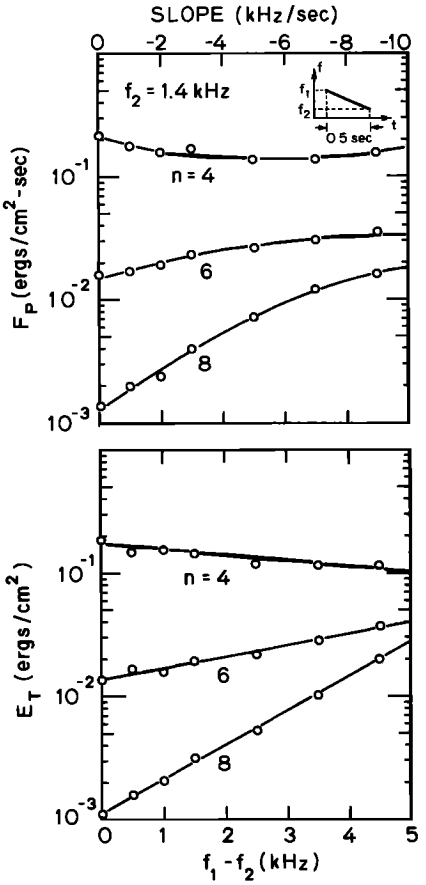

Fig. 8. Peak precipitation flux F_P and total deposited energy E_T as a function of $f_1 - f_2$ for signals whose input formats are given in Figure 6*b* and for three different values of n.

they decrease for the case of n=4. Note that input wave pulse containing higher frequency components can interact with particles of lower energies which are more populous in the assumed trapped distribution (5). Since the precipitation energy flux depends not only on the number of particles precipitated but also on their energies, it then is a function of the falloff with the energy of the trapped particle distribution function.

From Figure 8 it can be concluded that for $n \simeq 5$, F_P and E_T become independent of the frequency range of the input wave, a result that is consistent with the finding by [*1*] that for $f < 0.5 f_H$, both F_P and E_T increase with decreasing frequency for n=4, while they decrease for the case of n=6 and 8, indicating that the energy flux is approximately proportional to v^{5-n}.

Positive and Negative Slopes

We now consider the pulses of Figure 6*c* having a fixed input duration and center frequency but covering varying ranges of frequencies. Figure 9 shows results for a pulse of duration 0.5 s and center frequency 5.1 kHz for $f - t$ slopes of 0 to ±6 kHz/s, assuming n=6 in (5). The lower panel shows the integrated energy E_T as a function of slope. E_T is symmetric around zero slope up to ±5 kHz, which is consistent with the earlier observation that total energy precipitation is about the same for the riser and the faller. The integrated energy density is larger for the signals with higher slope, because they can interact with particles of both higher and lower energies and for a n=6 distribution the contribution of lower energy particles is more significant. It is thus expected that E_T would be larger for larger $f - t$ slopes due to the v^{5-n} dependence of the energy flux mentioned above.

The variation of peak flux with slope, as shown in the upper panel of Figure 9, is more complicated. It is found that the peak flux is decreasing with positive slope while it is increasing with negative slope. Due to the dispersion of the variable frequency wave, the wave intensity of each frequency component of the propagating wave pulse varies along the field line as described in the appendix. For the n=6 distribution the higher frequency components are more important, as discussed in connection with Figure 8; therefore we expect this part of the wave packet to have a greater effect on the peak flux level. Along the L=4 field line the group delay generally increases for frequencies higher than 5.1 kHz, which is the center frequency in this case since the nose frequency corresponding to our magnetospheric model and parameters is 5.05 kHz. Therefore for the risers the upper frequency portion of the pulse will generally spread as it propagates, causing the corresponding wave intensity to decrease. This effect is more pronounced for the pulse of higher slope, which contains higher frequency components. It thus results in the decrease in peak flux versus positive slope shown in Figure 9. The same argument accounts for the increase with respect to the increasing negative slope of the peak flux, since for the fallers the upper portion of the signal gets compressed instead of being lengthened. This difference between signals with positive and negative slopes also explains the smaller rate of increase in the total flux as a function of slope for the risers compared to that for the fallers, as seen in the lower panel of Figure 9.

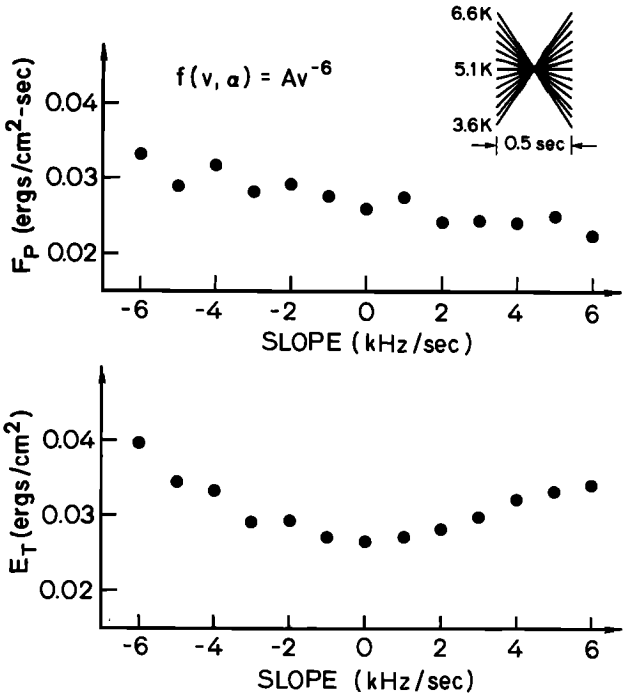

Fig. 9. Peak precipitation flux F_P and total deposited energy E_T as a function of slope for signals whose input formats are given in Figure 6*c*. The trapped particle distribution is assumed to be that with n=6.

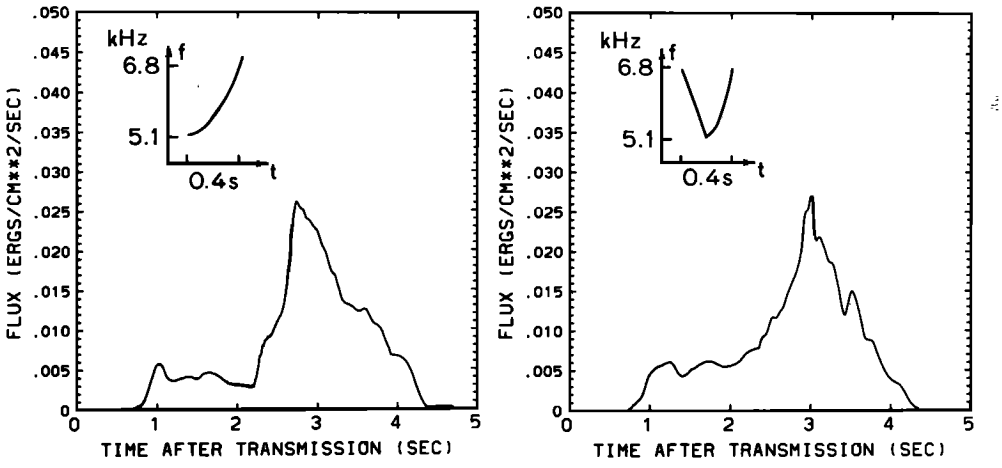

Fig. 10. Precipitated energy fluxes versus time for the emissionlike and the hooklike signals.

The results presented in this section indicate that although the temporal shape of the transient precipitation pulse induced by a variable frequency signal depends upon the location of its principle interaction region (i.e., the slope df/dt), there is little difference in total deposited energy E_T or peak flux F_P induced by signals with different $f-t$ slopes. When there are significant differences, as in the case of Figure 8, these are controlled more by the falloff in energy of the trapped particle distribution function (i.e., n) than by any other parameter.

6. Application to Typical Coherent Magnetospheric Signals

In this section we apply our formulation to estimate the precipitation induced by some signals with varying df/dt, namely, a typical triggered emission, a hook, and a lightning-generated whistler.

Emission and Hook

We first consider two signals with input $f-t$ formats as depicted in Figure 10. Both signals have $f_1 = 5.1$ kHz and f_2=6.8 kHz as their lowest and highest frequencies, respectively, and an input duration t_{PL}=0.4 s. One of them has an input $f-t$ format with a parabolic variation defined by $f = f_1+(f_2-f_1)(t/t_{PL})^2$ such that $f = f_1$ at $t = 0$ and $f = f_2$ at $t = t_{PL}$. When observed at the conjugate site, this signal would more closely resemble the typical triggered emission than would a signal with linear $f-t$ format. The input $f-t$ format for the other signal is constructed from a combination of a falling linear ramp of duration $t_{PL}/2$ and a parabolic signal of duration $t_{PL}/2$ defined by $f = f_1+(f_2-f_1)[2(t-t_{PL}/2)/t_{PL}]^2$, such that this signal would resemble a hook when observed at the conjugate point.

Our purpose here is to compare the precipitation fluxes induced by these two more complex signals with that due to a linear ramp covering the same frequency range and time duration (and therefore having the same input total energy), namely, the 0.4-s riser of Figure 7. Figure 10 shows the transient precipitation responses of the emissionlike and hooklike signals. It is found that the integrated energy densities of these three cases are about the same. This result is consistent with the previous comparisons between risers and fallers and shows that irrespective of the details of the $f-t$ format, input wave pulses having a fixed duration and covering the same frequency range would precipitate the same amount of electron energy during one-pass interactions with the trapped energetic particles under the condition of moderate wave intensities ($B_w \leq 10$ pT).

Although the integrated energy densities are the same, the temporal variations of the precipitation pulses are different for these three cases. The peak flux for the hooklike case is found to be 15% higher than the linear ramp case and about the same as the emissionlike case. This can be understood from the fact that the variation of the resonance velocity along the field line depends strongly on the $f-t$ format.

It should be noted that the above two signals have been assumed to originate at 1000 km altitude and propagate along the field line without growth or damping. In the more realistic case where these waves are generated near the magnetic equator, their induced precipitated energy fluxes would be reduced based on the same argument in the discussion of wave growth effect for the cases of riser and faller shown in Figure 4.

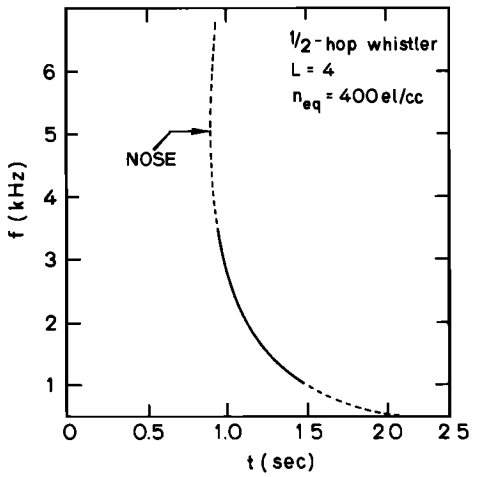

Fig. 11. The frequency-time format observed at the equatorial plane of a lightning-generated signal propagating on the L=4 field line, termed a half-hop whistler. The solid segment represent that portion considered in the calculation of particle precipitation.

Natural Whistler

Here we consider the case of a lightning-generated whistler originating in the southern hemisphere and propagating northward along the L=4 field line. We calculate the transient precipitated flux induced by this simulated one-hop whistler. For simplicity, only that portion of the lightning stroke in the frequency range of 3.5 kHz to 1.0 kHz is considered, as shown in Figure 11. The frequency of the leading edge of the propagating whistler packet will always be 3.5 kHz since the assumed frequency range is below the nose frequency of 5.05 kHz in our model. The magnetospheric parameters along the L=4 line were taken to be the same as in the previous sections.

The input energy of the lightning impulse is taken as equivalent to that contained in a 0.5-s constant frequency wave pulse at half the equatorial gyrofrequency and having an equatorial wave intensity of 5 pT. As the input lightning-generated wave travels along the field line, the signal is dispersed and the wave magnetic field intensity varies accordingly (see appendix). If we observe this whistler at the geomagnetic equatorial plane, the signal format in the $f-t$ domain according to our model magnetosphere will be that represented by the solid segment in Figure 11. The front and tail ends of the wave packet arrive at t=0.96 s and 1.49 s, respectively, so the equatorial pulse duration is 0.53 s. The dashed curve in Figure 11 shows the arrival times of frequency components other than those considered in our case up to half of the equatorial gyrofrequency. The arrow indicates the nose frequency.

Figure 12 shows the resonance velocity curves for a particular particle with equatorial parallel velocity of 1.2×10^8 m/s and at a pitch angle of $\alpha_{eq} = 5.5°$ corresponding to an energy of 47 keV. The dashed curve shows the adiabatic parallel velocity along the field line. Each curve segment in Figure 12 starts at the latitude at which the given particle

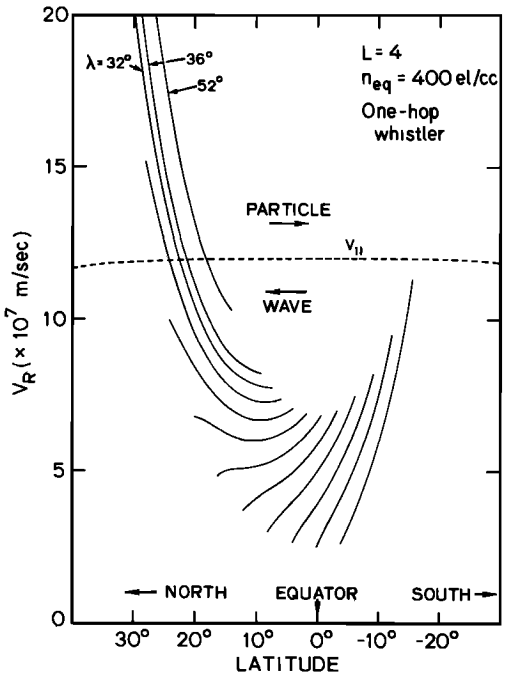

Fig. 12. The v_R curves for a particle whose adiabatic parallel velocity is given by the dashed curve and the propagating whistler signal described in Figure 11.

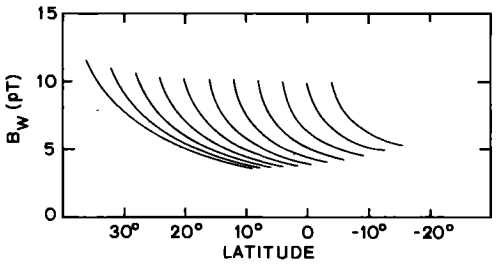

Fig. 13. The wave amplitude variation versus latitude experienced by the test particle shown in Figure 12 as it travels within the whistler wave packet. Each curve corresponds to a v_R curve in Figure 12.

encounters the leading edge of the whistler and ends at the latitude at which this particle exits the whistler wave packet. As the whistler propagates toward the north, it continually meets particles of this given equatorial velocity and the corresponding resonance curve as determined by (2) varies from step to step. It is noted that the envelope formed by the starting points of all the v_R curves is the resonance velocity curve corresponding to a constant-frequency wave at the leading frequency of the whistler or 3.5 kHz. Similarly, the v_R curve corresponding to the tail frequency can be obtained by forming the envelope of the end points of the v_R curves. Since the whistler has negative slope in the $f-t$ domain, it is expected that the resonance velocity curves will show zero gradients in some portion of the field line in the northern hemisphere [*Helliwell*, 1970], as is the case in Figure 11. As the whistler propagates and its front end reaches higher latitudes, the minimum in v_R is due to the lower frequency part of the whistler. Since the lower frequency portion has smaller slope, as can be seen from Figure 11, the minimum is gradually shifted toward the equator.

Since the resonance point is determined by the intersection of the v_R curve and the $v_{||}$ curve, the particle shown in Figure 12 will interact with the whistler between 15° and 25° latitudes. But since v_R varies rapidly in this region, the cumulative pitch angle scattering of the particle is not large in comparison to the interaction at locations where the gradients of the v_R curves are smaller. This has been confirmed by our computation and in fact the parallel velocity and the corresponding energy of this particle, which suffers an equatorial pitch angle scattering less than 0.1°, have been used as the upper limit of the test particle distribution in our calculation. For particles of lower energy, each v_R curve will span a shorter range of latitude due to the smaller parallel velocities; however, its shape will remain qualitatively similar. Thus we conclude from Figure 12 that particles with parallel velocity (energy) between 5×10^7 (7.3 keV) and 8×10^7 m/s (19.4 keV) will interact strongly with the whistler in the vicinity of 10° latitude in the northern hemisphere and consequently play a major role in the contribution to the precipitation as will be demonstrated later.

Figure 13 shows the wave amplitude variation experienced at each step by the test particle shown in Figure 12 as it travels within the wave packet. Since the input energy density of the lightning impulse is assumed to be uniformly distributed over all frequency components, the lower frequencies have lower wave intensities because of greater dispersion.

The transient precipitation flux induced by this one-hop whistler is shown in Figure 14, assuming n=6 in (5). The

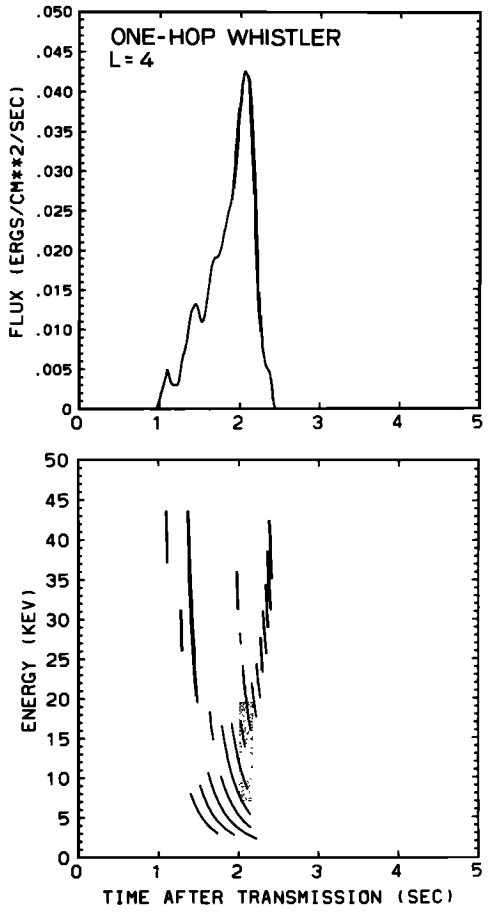

Fig. 14. The top panel shows the transient precipitated energy flux versus time for the whistler described in Figure 11. The bottom panel shows the energy versus arrival time at the wave injection point of the precipitating particles. The shaded region indicates the locations of those particles that undergo strong interactions with the whistler at around 10° latitude in the northern hemisphere.

energy diagram in the lower panel shows that the energy of the precipitated particles ranges from about 2 keV up to 45 keV. The upper panel indicates that the peak flux arrives about 2 s after the injection of the impulse energy and is constituted by particles at lower energies as shown in the lower panel. Those particles which were pointed out to undergo strong interactions with the whistler at around 10° latitude in the northern hemisphere in the discussion of Figure 12 and whose locations in the energy diagram are indicated by the shaded region in Figure 14 clearly contribute to the main portion of the precipitated flux.

The integrated energy density E_T induced by this whistler is 0.023 ergs/cm^2 for an input wave energy density that was taken to be the same as in the cases of Figures 8 and 9. We have found that for an n=6 distribution, E_T is strongly dependent on the highest frequency component of the input signal, at least in the cases with linear input df/dt. If we compare E_T of the whistler with a linear ramp with the same upper frequency in Figure 8*b*, we find that the integrated energy density precipitated by the whistler is comparable to that of the linear ramp. This result clearly indicates that E_T is primarily determined by the input energy of the wave. The peak flux of the whistler, being $F_P = 0.42$ ergs/cm^2 s, is found to be higher than those in Figure 8*a* due to the relatively narrower range in the arrival times of the precipitating particles.

It is interesting to note that substantial leverage is involved in the transient wave-induced precipitation process. For example, in the whistler case the input wave energy density is 8.3×10^{-6} ergs/cm^2; comparing with $E_T = 0.023$ ergs/cm^2, the leverage is ≈3000. In other words, the energy density of the precipitating signal can be and in most cases is much larger than the energy density of the wave. This result illustrates the fact that the interacting wave essentially acts as a means for converting particle perpendicular energy into parallel energy (i.e., lowering the pitch angle) with relatively small energy exchange. The precipitated energy then is mostly due to the existing kinetic energy of the radiation belt particles.

7. Summary and Concluding Remarks

We have studied the energetic electron precipitation out of the magnetosphere due to the gyroresonant interactions of these particles with coherent VLF waves with slowly varying frequency. The effect of the frequency-time format of the input signal on the properties of the transient precipitated energy flux was examined.

Our results show that under conditions of moderate wave intensities ($B_w < 10$ pT at L=4), slowly varying frequencies, and the assumptions that the wave energy is conserved during propagation between the two hemispheres, the total deposited energy density E_T is the same at least to first order for coherent wave pulses having the same input energy and frequency range. Thus for coherent slowly varying signals, E_T is not strongly dependent on the $f - t$ format of the input signal (riser, faller, or other more complex shapes discussed in the previous sections), although the temporal evolution and the peak value of the precipitation flux may vary due to the different combinations of the wave and particle travel times.

To account for observed wave growth effects, we have considered the cases in which the wave growth takes place in the vicinity of the phase equator or within the principal interaction region. It was found that for cases when such growth is present, the riser is more efficient than the faller in inducing particle precipitation due to the different locations of their principal interaction regions. The concept of principal interaction region was clearly demonstrated by showing representative resonance velocity curves for both risers and fallers.

Our results indicate that in the unamplified cases (neglecting wave growth) the total deposited energy density E_T and peak flux F_P induced by input signals of varying frequency exhibit little difference from those of the monochromatic cases discussed by [*1*]. However, when wave growth around the principal interaction region (assumed to be located at the geomagnetic equator for constant frequency waves) is taken into account, the precipitation efficiency for the monochromatic cases is between that of the riser and faller.

In the previous section we have shown that a substantial energy leverage of ≈3000 is involved in the transient wave-induced precipitation process for the whistler case. This result clearly reflects one feature of the cyclotron resonance interaction in that pitch angle changes of particles are basically changes of the direction of momentum caused mainly

by the wave magnetic field and do not require a large amount of energy exchange.

The precipitated energy flux levels for the cases considered in this paper ($\Phi_E = 10^8$ el/cm^2 ster s keV for E=1 keV, B_w=5 pT) range from 10^{-3} to 10^{-1} ergs/cm^2 s for particles with energy less than 50 keV, with those obtained from v^{-6} trapped distribution being in the order of 10^{-2} ergs/cm^2 s. These levels are directly proportional to Φ_E and B_w, as discussed below. Both of these parameters can vary by two orders of magnitude depending on the conditions involved. When the values of Φ_E and B_w can be determined, our results can be scaled (up or down) to find the absolute flux levels. These can then be compared with the background drizzle-type precipitation levels at midlatitudes that are in the range of 10^{-6}–10^{-4} ergs/cm^2 s [*Voss and Smith*, 1980] and the detectability of the wave-induced fluxes by presently available instruments can be assessed [*Doolittle*, 1982; *Inan et al.*, 1982].

In the following we summarize and discuss the roles of the energetic particle distribution, the wave intensity variation, and the wave frequency variation in our results.

The Energetic Particle Distribution

We have assumed an initial particle distribution function defined by (5). The coefficient A in (5) is proportional to the differential energy spectrum Φ_E of the trapped particles, as discussed by [*I*]. In our calculations we used $\Phi_E = 10^8$ el/cm^2 s ster keV for particles with energy E=1 keV and at $\alpha = 90°$ pitch angle. This value is typical of the flux levels outside and just inside the plasmapause during geomagnetically disturbed times [*Schield and Frank*, 1970; *Anderson*, 1976] and has been taken as a reference value in previous work [*Inan et al.*, 1978; *I*]. Under other conditions, Φ_E could be as low as 10^5–10^6 el/cm^2 ster s keV [*Lyons and Williams*, 1975]. The precipitated energy fluxes given in this paper are directly proportional to Φ_E. Thus the energy density values given in Figures 3–14 need to be scaled down for other values of Φ_E.

Throughout this paper we have assumed an isotropic distribution for which $g(\alpha) = 1$ in (5) for $\alpha > \alpha_{lc}$. Anisotropic distributions are more likely to occur in the magnetosphere [*Lyons and Williams*, 1975]. The cases in which $g(\alpha)$ drops to zero at $\alpha = \alpha_{lc}$ gradually rather than sharply were discussed by [*I*] and were shown to result in reduced flux levels depending on the slope of $g(\alpha)$ at $\alpha = \alpha_{lc}$. Thus the effect of anisotropy is easily accountable and is not essential to our discussion of the influence of the input signal format on induced precipitation.

For most of the results presented in this paper we have assumed n=6 in (5). The dependence of precipitation on n was discussed in connection with Figures 5 and 8. For lower n values, the contribution of higher energy particles is more important and a double peak tends to form in the flux pulse (Figure 5), as in the fixed frequency cases of [*I*]. The results of Figure 8 confirm the finding of [*I*] that the energy flux is approximately proportional to v^{5-n}, since they show that for $n \simeq 5$ the precipitated energy flux is independent of the frequency range and thus the $f-t$ format of the input signal as long as the input wave energy is fixed.

The Wave Intensity Variation

In calculating the wave-induced perturbations of the energetic particle population, we have assumed that the wave structure is known as a function of space and time and have not directly included the effects on the wave of the electromagnetic fields generated by the perturbed particles. This amounts to, in effect, assuming that the fields radiated by the perturbed particles are negligible, as in the case of an unamplified wave, or that this effect has been included in the model chosen for the wave structure. Justification for this assumption for the purpose of computing the precipitated flux is given in earlier work [*I*; *Inan et al.*, 1982]. To indirectly account for the effect of wave growth in some cases (Figure 4), we have presumed that the signal undergoes an amplification of at least 20 dB across the principal interaction region. Experimental and theoretical evidence suggest that the region of temporal growth is within a few degrees of the geomagnetic equator [*Helliwell*, 1967; *Helliwell and Katsufrakis*, 1974]. Any change in the wave amplitude structure will thus occur over a relatively small portion of the field line. The effect of such a nonuniform amplitude variation on the total precipitated flux can be indirectly accounted for by choosing a suitable wave structure.

The wave amplitude variation along the field line due to the dispersive and inhomogeneous nature of the medium is discussed in the appendix. We have found that this consideration is essential in the calculation of precipitation due to variable frequency signals.

We have assumed moderate wave intensities ($B_w \leq 10$ pT at L=4) in most of the calculations in this paper. It was demonstrated by [*I*] that this range of wave intensities is in the linear regime for the parameters used and the precipitated flux is linearly proportional to B_w in this regime. The typical unamplified intensities of manmade VLF transmitter signals in the magnetosphere fall in the linear range [*Inan et al.*, 1977; *Bell et al.*, 1981]. However, the signal level might exceed this moderate intensity limit after amplification and triggering [e.g., *Burtis and Helliwell*, 1975]. For these higher field intensity cases the trapping of particles may play a more significant role so that the precipitated flux can not simply be scaled up or down proportionally with B_w.

The Wave Frequency Variation

The frequency-time formats of the signals studied in this paper are all of monotonic variation except in the case of the hook. Thus a particle interacting with any of these signals will have either one or two resonance points which are the intersections of the v_R segment and the particle's $v_{||}$ curve, as is represented in Figures 1, 2, and 12. In the neighborhood of the resonance point, the variation of the cyclotron phase ϕ as given by (1) should be slow ($\ddot{\phi} \simeq 0$) enough that the interaction time (defined as the period in which ϕ goes through $\pm\pi/2$) is long enough for significant cumulative pitch angle change. In this paper, 0.1° change in equatorial pitch angle at L=4 was taken as the criterion.

For the case of variable frequency wave, the variation of ϕ depends not only on the inhomogeneity of the medium (i.e., the gradient of the local electron gyrofrequency) but also on the spatial or temporal variation of ω seen by the particle in the vicinity of the resonance point, according to (1). If the variation of $|\omega_H - \omega|$ is much faster than that of ω_H along the particle trajectory, being equivalent to moving the resonance region from the geomagnetic equator for the case of interacting with constant frequency wave, the resonance interaction time for individual particles and thus

the total scattering would accordingly be reduced. For the cases considered in this paper the wave frequency variation within $\pm 20^\circ$ latitude of the equator has been slow enough such that a large number of the trapped particles could undergo significant pitch angle scattering ($\Delta\alpha_{eq} > 0.1^\circ$) there and be precipitated into the loss cone. It is worthwhile pointing out that a lightning-generated whistler has a very large rate of change of frequency with time at the source point, however, due to the dispersion, it is slowly varying in frequency near the geomagnetic equator, as implied in Figures 12 and 13.

APPENDIX: WAVE AMPLITUDE VARIATION

In our model a short VLF wave pulse is assumed to enter into the magnetosphere at 1000 km altitude at time t=0 and is assumed to propagate longitudinally ($\mathbf{k}||\mathbf{B}_0$) in a duct along the earth's magnetic field line.

For a monochromatic wave pulse the temporal pulse duration does not change during propagation, neglecting the possible distortion of the front and tail ends of the pulse [*Chang and Helliwell*, 1980]. If no loss of energy is assumed, the power flow along the duct is then constant. However, the power density varies, since the cross-sectional area of the duct is modeled as being inversely proportional to the static magnetic field intensity B_0 or to the cold plasma electron frequency ω_H, assuming that the whistler mode wave is the superposition of a large number of rays that fill up the duct. In this slowly varying medium, the variation of the wave magnetic field intensity B_w along the field line can then be expressed as

$$B_w = B_{weq}(\omega_H k/\omega_{Heq} k_{eq})^{1/2} \tag{A1}$$

since ${B_w}^2$ is proportional to the power density and the refractive index μ ($=ck/\omega$). In (A1), ω_H and k are local values, ω_{Heq} and k_{eq} are the equatorial values, B_{weq} is the equatorial wave intensity, c is the speed of light in free space, and ω is the angular wave frequency.

For a variable frequency signal the pulse duration varies due to the dispersive nature of the medium. The wave power density and so the wave intensity will depend on this additional factor. The local group velocity of a wave component of frequency f along the field line is given [*Helliwell*, 1965] by

$$v_g = 2c\frac{f^{1/2}(f_H - f)^{3/2}}{f_P f_H} \tag{A2}$$

where $f_P = \omega_P/2\pi$ and $f_H = \omega_H/2\pi$ are the local plasma frequency and gyrofrequency, respectively, and ${\omega_P}^2 \gg {\omega_H}^2$ has been assumed. The travel time, or the group delay, of this frequency component from the injection point to a point with coordinate z along the field line can be expressed as

$$t_g(f,z) = \int_{1000\text{km}}^{z} \frac{dz}{v_g} = \frac{1}{2c}\int_{1000\text{km}}^{z} \frac{f_P f_H}{f^{1/2}(f_H - f)^{3/2}}\,dz \tag{A3}$$

Consider one component of a variable frequency signal with frequency f which is injected into the field line at time t. An adjacent frequency component $f + \Delta f$ is injected at time $t + \Delta t$. $\Delta f/\Delta t$ is then the slope in the $f - t$ domain of the input signal at frequency f. The components f and $f + \Delta f$ will travel to the point z at times t' and $t' + \Delta t'$, respectively. From (A3), $\Delta t'$ is then given by

$$\Delta t' = \Delta t + t_g(f + \Delta f, z) - t_g(f, z) \tag{A4}$$

Note that Δt and $\Delta t'$ may have different signs; however, in this paper we do not treat this case. The difference in group delay can be approximated by

$$t_g(f + \Delta f, z) - t_g(f, z) = \frac{\partial t_g(f,z)}{\partial f}\Delta f \tag{A5}$$

where $\partial t_g(f,z)/\partial f$ is the slope of the $t_g(f)$ versus f curve measured at f and can be derived from (A3) as

$$\frac{\partial t_g(f,z)}{\partial f} = \frac{1}{2c}\int_{1000\text{km}}^{z} \frac{f_P f_H}{f^{1/2}(f_H - f)^{3/2}} \cdot\left[\frac{3}{2}\frac{1}{(f_H - f)} - \frac{1}{2f}\right] dz \tag{A6}$$

Consequently, (A4) can be rewritten as

$$\frac{\Delta t'}{\Delta t} = 1 + \frac{\partial t_g(f,z)}{\partial f}\frac{\Delta f}{\Delta t} \tag{A7}$$

If the energy contained between $f + \Delta f$ and f is conserved, the local power flow or power density corresponding to f is inversely proportional to its duration Δt. The wave intensity at z of this frequency component will accordingly be modified by the factor $(\Delta t/\Delta t')^{1/2}$ in addition to that given by (A1). Note that we have assumed that $\Delta t'$ does not go to zero. The complete expression for computing the wave intensity variation along the field line using the equatorial wave intensity as a reference is then given by

$$B_w(f,z) = B_{weq}(f) \cdot\left[\frac{\omega_H(z)k(f,z)(1 + [\partial t_g(f,z_{eq})/\partial f][\Delta f/\Delta t])}{\omega_{Heq} k_{eq}(f)(1 + [\partial t_g(f,z)/\partial f][\Delta f/\Delta t])}\right]^{1/2} \tag{A8}$$

where f and z indicate the dependence of the different quantities on the frequency and position along the field line, respectively, eq represents equatorial values, and $\Delta f/\Delta t$ is the slope of the signal in the input $f - t$ domain. Equations (A7) and (A8) are used in all of the model computations reported in this paper.

Acknowledgments. We wish to acknowledge the many valuable discussions we have held with our colleagues at the Radioscience Laboratory. This research was supported by the National Aeronautics and Space Administration under contract NGL-05-020-008 and by the National Science Foundation under contract ATM-80-18248. The computer calculations were made on the CDC7600 and CRAY-1 computers of the National Center for Atmospheric Research (NCAR) in Boulder, Colorado. Our use of this facility was made possible by a Computer Resources grant from NCAR.

The editor thanks H. C. Koons and another referee for their assistance in evaluating this paper.

REFERENCES

Anderson, R. R., Wave particle interactions in the evening magnetosphere during geomagnetically disturbed periods, Ph.D. thesis, Univ. of Iowa, Iowa City, 1976.

Angerami, J. J., and D. L. Carpenter, Whistler studies of the plasmapause in the magnetosphere, 2, Equatorial density and total tube electron content near the knee in magnetospheric ionization, *J. Geophys. Res., 71,* 711, 1966.

Bell, T. F., U. S. Inan, and R. A. Helliwell, Nonducted coherent VLF waves and associated triggered emissions observed on the ISEE-1 satellite, *J. Geophys. Res., 86,* 4649, 1981.

Burtis, W. J., and R. A. Helliwell, Magnetospheric chorus: Amplitude and growth rate, *J. Geophys. Res., 80,* 3265, 1975.

Carpenter, D. L., and J. W. LaBelle, A study of whistlers correlated with bursts of electron precipitation near $L=2$, *J. Geophys. Res., 87,* 4427, 1982.

Chang, D. C. D., and R. A. Helliwell, VLF pulse propagation in the magnetosphere, *IEEE Trans. Antennas Propagat., AP28,* 170, 1980.

Chang, H. C., and U. S. Inan, Quasi-relativistic electron precipitation due to interactions with coherent VLF waves in the magnetosphere, *J. Geophys. Res., 88,* 318, 1983.

Dingle, B., and D. L. Carpenter, Electron precipitation induced by VLF noise bursts at the plasmapause and detected at conjugate ground stations, *J. Geophys. Res., 86,* 4597, 1981.

Doolittle, J. H., Modification of the ionosphere by VLF wave-induced electron precipitation, Ph.D. thesis, Radiosci. Lab., Stanford Electron. Labs., Stanford Univ., Stanford, Calif., 1982.

Dysthe, K. B., Some studies of triggered whistler emissions, *J. Geophys. Res., 76,* 6915, 1971.

Foster, J. C., and T. J. Rosenberg, Electron precipitation and VLF emissions associated with cyclotron resonance interactions near the plasmapause, *J. Geophys. Res., 81,* 2183, 1976.

Helliwell, R. A., *Whistlers and Related Ionospheric Phenomena,* Stanford University Press, Stanford, Calif., 1965.

Helliwell, R. A., A theory of discrete VLF wave emissions from the magnetosphere, *J. Geophys. Res., 72,* 4773, 1967.

Helliwell, R. A., Intensity of discrete VLF emissions, in *Particles and Fields in the Magnetosphere,* edited by B. M. McCormac, p. 292, D. Reidel, Hingham, Mass., 1970.

Helliwell, R. A., and J. P. Katsufrakis, VLF wave injection into the magnetosphere from Siple Station, Antarctica, *J. Geophys. Res., 79,* 2511, 1974.

Helliwell, R. A., J. P. Katsufrakis, and M. L. Trimpi, Whistler-induced amplitude perturbation in VLF propagation, *J. Geophys. Res., 78,* 4679, 1973.

Helliwell, R. A., S. B. Mende, J. H. Doolittle, W. C. Armstrong, and D. L. Carpenter, Correlations between λ4278 opticqal emissions and VLF wave events observed at $L\sim4$ in the Antarctic, *J. Geophys. Res., 85,* 3376, 1980.

Imhof, W. L., E. E. Gaines, and J. B. Reagan, Observations of multiple, narrow energy peaks in electrons precipitating fom the inner radiation belt and their implications for wave-particle interactions, *J. Geophys. Res., 86,* 1591, 1981*a*.

Imhof, W. L., R. R. Anderson, J. B. Reagan, and E. E. Gaines, The significance of VLF transmitters in the precipitation of inner belt electrons, *J. Geophys. Res., 86,* 11225, 1981*b*.

Imhof, W. L., J. B. Reagan, H. D. Voss, E. E. Gaines, D. W. Datlowe, J. Mobilia, R. A. Helliwell, U. S. Inan, J. P. Katsufrakis, and R. G. Joiner, Direct observation of radiation belt electrons precipitated by controlled injection of VLF signals from a ground-based transmitter, submitted to *Geophys. Res. Lett.,* 1983.

Inan, U. S., Non-linear gyroresonant interactions of energetic particles and coherent VLF waves in the magnetosphere, *Tech. Rep. 3414-3,* Radiosci. Lab., Stanford Electron. Labs., Stanford, Calif., 1977.

Inan, U. S., T. F. Bell, D. L. Carpenter, and R. R. Anderson, Explorer 45 and Imp 6 observations in the magnetosphere of injected waves from the Siple Station VLF transmitter, *J. Geophys. Res., 82,* 1177, 1977.

Inan, U. S., T. F. Bell, and R. A. Helliwell, Nonlinear pitch angle scattering of energetic electrons by coherent VLF waves in the magnetosphere, *J. Geophys. Res., 83,* 3235, 1978.

Inan, U. S., T. F. Bell, and H. C. Chang, Particle precipitation induced by short-duration VLF waves in the magnetosphere, *J. Geophys. Res., 87,* 6243, 1982.

Koons, H. C., B. C. Edgar, and A. L. Vampola, Precipitation of inner zone electrons by whistler mode waves from VLF transmitters UMS and NWC, *J. Geophys. Res., 86,* 640, 1981.

Lyons, L. R., and D. J. Williams, The quiet time structure of energetic (35-560 keV) radiation belt electrons, *J. Geophys. Res., 80,* 943, 1975.

Roberts, C. S., Electron loss from the Van Allen zones due to pitch angle scattering by electromagnetic disturbances, in *Radiation Trapped in the Earth's Magnetic Field,* edited by B. M. McCormac, pp. 403–421, D. Reidel, Hingham, Mass., 1966.

Roederer, J. G., *Dynamics of Geomagnetically Trapped Particles,* Springer, New York, 1970.

Rosenberg, T. J., R. A. Helliwell, and J. P. Katsufrakis, Electron precipitation associated with discrete very-low-frequency emissions, *J. Geophys. Res., 76,* 8445, 1971.

Rosenberg, T. J., J. C. Siren, D. L. Matthews, K. Marthinsen, J. A. Holtet, A. Egeland, D. L. Carpenter, and R. A. Helliwell, Conjugacy of electron microbursts and VLF chorus, *J. Geophys. Res., 86,* 5819, 1981.

Schield, M. A., and L. A. Frank, Electron observations between the inner edge of the plasma sheet and the plasmasphere, *J. Geophys. Res., 75,* 5401, 1970.

Vampola, A. L., and G. A. Kuck, Induced precipitation of inner zone electrons, 1. Observations, *J. Geophys. Res., 83,* 2543, 1978.

Voss, H., and L. G. Smith, Global zones of energetic particle precipitation, *J. Atmos. Terr. Phys., 42,* 227, 1980.

(Received December 21, 1982;
revised April 11, 1983;
accepted April 26, 1983.)